INTERFACE

rsif.royalsocietypublishing.org

Research

Check for updates

Cite this article: Zhang L, Stepan G, Insperger T. 2018 Saturation limits the contribution of acceleration feedback to balancing against reaction delay. *J. R. Soc. Interface* 20170771.
http://dx.doi.org/10.1098/rsif.2017.0771

Received: 17 October 2017
Accepted: 9 January 2018

Subject Category:
Life Sciences – Mathematics interface

Subject Areas:
biomechanics

Keywords:
human balancing, reaction delay, acceleration feedback, saturation, Hopf bifurcation

Author for correspondence:
Li Zhang
zhangli@nuaa.edu.cn

THE ROYAL SOCIETY
PUBLISHING

Saturation limits the contribution of acceleration feedback to balancing against reaction delay

Li Zhang[1], Gabor Stepan[2] and Tamas Insperger[2,3]

[1]State Key Laboratory of Mechanics and Control of Mechanical Structures, Nanjing University of Aeronautics and Astronautics, Nanjing 210016, People's Republic of China
[2]Department of Applied Mechanics, Budapest University of Technology and Economics, and
[3]Economics and MTA-BME Lendület Human Balancing Research Group, 1521 Budapest, Hungary

LZ, 0000-0001-6077-9093

A nonlinear model for human balancing subjected to a saturated delayed proportional–derivative–acceleration (PDA) feedback is analysed. Compared to the proportional–derivative (PD) controller, it is confirmed that the PDA controller improves local stability even for large feedback delays. However, it is shown that the saturated PDA controller typically introduces subcritical Hopf bifurcation into the system, which can also lead to falling for large enough perturbations. The subcriticality becomes stronger as the acceleration feedback gain increases or the saturation torque limit decreases. These explain some features of human balancing failure related to the increased reaction delay of inactive elderly.

1. Introduction

Standing and moving on two legs is an essential component of everyday human activities. The related instability in the dynamics of quiet standing has both advantages and disadvantages. On the one hand, standing in an unstable position improves the mobility in the sense that minimum control effort is needed to start moving in any desired direction. On the other hand, the control should be maintained continuously to stabilize the upright position. This balancing task is especially important at the beginning and at the end of our lives. Babies need a long learning process to stand up, while elderly people may have serious and even fatal injuries when they fall over. Research [1,2] has shown that falling is the leading cause for elderly peoples' injury, which poses both health and economic burden for the individual family and the whole society. It has also been recognized in [3] that more falls occur during standing and weight transferring than during walking. This draws the attention for the importance of possible perturbation levels in human balancing.

Because of the finite speed of signal propagation and processing in the central nervous system, time delays are intrinsic components of neural control and have a great influence on the stability of human balancing [4–10]. Helmholtz was the first (see [11]) who showed that the speed of signal propagation is one order of magnitude slower than the speed of sound. In addition to propagation time, signal processing also takes time especially for complex information sources like vision [12]. All these conductive and processing times lead to delays in the range of 0.1–1 s in the human motion control system [13]. Time delay, especially its processing part, increases with age for inactive elderly.

In case of quiet standing, primarily the vestibular system is used together with the mechanoreceptors and the proprioceptors. In these cases, the reaction time is estimated between 75 and 125 ms (see [14,15]) for healthy adults, but it is in the range of 153–177 ms for elders (see [16]). This reaction delay can be even longer for inactive elderly, tired and/or distracted persons. When the feedback mechanism relies also on the visual sensory information (see [17,18]), the reaction delay may increase up to 300 ms or even longer (see [19]). Presumably, all the above sensory information are used during quiet standing, resulting in a complex combination of the perceived signals provided by the different sensory organs associated with different conducting and processing delays. Therefore, reaction delay is a key component in studying human balance control.

Balancing abilities are often analysed using linearized dynamical models. However, nonlinearities are always present and can increase the complexity of the dynamical behaviours particularly as time delays become long. There are three major sources of nonlinearities: (i) geometric nonlinearity; (ii) sensory threshold; (iii) control force saturation. The geometric nonlinearity is mainly related to the torque induced by the gravitational force; this nonlinearity is usually neglected in the standard region of sway angles. The sensory threshold originates in a dead zone, which is a strong, small-scale nonlinearity. This nonlinearity has essential effects on the generation of micro-chaotic dynamics [20,21], but it has only slight effect on the stabilization of the large-scale system. During quiet standing, the active torque provided at the ankle has a limit according to the individual's muscle capacity. This saturation limit usually decreases with age for inactive people, which is possibly an essential component of the causes for the falling of the elderly, especially in case of unexpected perturbations. Therefore, torque saturation should be of concern for the balance control of the inactive elderly group.

Understanding the mechanism how humans maintain balance is a substantial task in brain research. Most interpretations are based on linear delayed proportional–derivative (PD) controllers [13,22–24]. These models have been developed as a kind of biomechanical analogies of position control of rigid body systems, like robots [25]. Linear PD controllers are still one of the most popular control strategies due to their simplicity and robustness [26] and they are widely used in control theory of time delay systems [27,28]. It is assumed that the human sensory system is able to perceive signals about the angular position and angular velocity of the human body. There are several studies in the specialist literature which explained how these signals are provided by the visual system [12], by the vestibular labyrinth [29] or by the proprioceptive inputs [30]. For the purpose of vibration control, the accelerometer has gained wide applications due to its low cost, small volume and light weight [28]. Recent research has indicated that angular acceleration signals might also be provided especially by the mechanoreceptive inputs through the tactile system [31]. Considering the large time delays in human control, the use of acceleration signals seems to be very advantageous in balancing [4]. It was shown there that proportional–derivative–acceleration (PDA) controllers was superior to the PD feedback by increasing the critical delay margin by approximately 40%.

A less feasible but still interesting way to improve balancing is the use of vertical periodic excitation at the ankle (see [32]), which uses the principle of parametric excitation as in the case of Kapitza's pendulum [33]. Although stabilization cannot be achieved only by parametric excitation due to the unilateral constraint between the foot and the vibrating platform, it can still contribute to the stabilization by feedback control (see [34,35]).

This paper deals with a balancing model based on a delayed PDA controller with geometric and saturation nonlinearities. It is shown that saturation nonlinearity has a counterintuitive effect on the dynamics of balancing with PDA controllers in contrast with the PD controllers. This result provides new insights into the causes of increased number of fall overs of inactive elderly people.

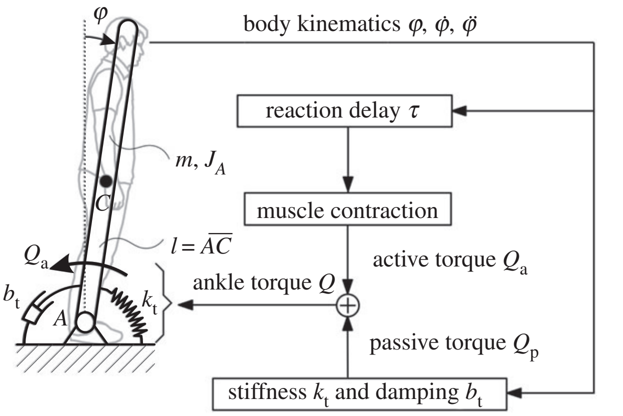

Figure 1. Neural-mechanical model of balancing in sagittal plane.

The structure of the paper is as follows. First, a neural–mechanical model is presented for human balancing in the sagittal plane involving reaction delay and saturation of the active torque at the ankle. The governing equation takes the form of a nonlinear neutral delay differential equation (NDDE). In §3, linear stability is analysed, stability charts are constructed and critical time delays are identified as a function of the acceleration gain. In §4, the nonlinear analysis is performed, namely, the Hopf bifurcation is studied via symbolic normal form calculation and also via the method of multiple scales. The results are confirmed by a numerical path-following method. A case study is presented with biophysically plausible human parameters in §5, which leads to the conclusions on the role of acceleration gains and saturation nonlinearity in human balancing.

2. Neural–mechanical model

The neural–mechanical model of human balancing in the sagittal plane is depicted in figure 1. The human body is modelled as an inverted pendulum with mass m, moment of inertia J_A with respect to pivot A, while l stands for the distance between the centre of gravity C and pivot A. The body is controlled by the ankle torque Q at joint A. The ankle torque Q consists of a passive torque Q_p and an active torque Q_a. The passive torque Q_p depends on the stiffness and damping of the ankle joints, which are modelled by a torsional spring of stiffness k_t and a torsional dashpot of damping b_t. As shown by Loram & Lakie [36], the ankle stiffness k_t is provided by the foot, Achilles' tendon and aponeurosis, and it is not large enough to maintain balance against the gravitational torque. Therefore, the additional active control torque Q_a is needed during quiet standing, which is generated by the contractile elements of the ankle muscles [37]. This torque is regulated by the central nervous system based on the sensory signals about rotation angle φ, angular velocity $\dot\varphi$ and angular acceleration $\ddot\varphi$ of the human body. The governing equation of this model can then be expressed in the form

$$J_A\ddot\varphi - mgl\sin\varphi = -Q(t), \tag{2.1}$$

where

$$Q(t) = Q_p(t) + Q_a(t), \tag{2.2}$$

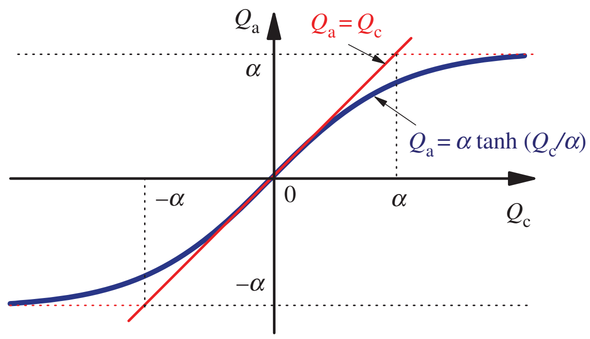

Figure 2. Saturated active control torque Q_a versus linear active control torque Q_c. (Online version in colour.)

with the passive torque defined as

$$Q_p(t) = b_t\dot{\varphi} + k_t\varphi. \tag{2.3}$$

The saturated active torque $Q_a(t)$ is assumed in the nonlinear form

$$Q_a(t) = \alpha \tanh\left(\frac{1}{\alpha} Q_c(t)\right), \tag{2.4}$$

where α denotes the limit of the active torque and its linear part is

$$Q_c(t) = K_p\varphi(t-\tau) + K_d\dot{\varphi}(t-\tau) + K_a\ddot{\varphi}(t-\tau), \tag{2.5}$$

with K_p, K_d and K_a being the positive proportional, derivative and acceleration gains, respectively. The delayed signals of angle φ and angular velocity $\dot{\varphi}$ are provided by the vestibular system and proprioceptors, while the angular acceleration $\ddot{\varphi}$ signal is related to the information coming from the mechanoreceptors according to Newton's Second Law [4]. The saturation effect is shown in figure 2, where the active control torque Q_a tends to the saturation torque limit α as Q_c increases.

For simplicity, the delayed terms $\varphi(t-\tau)$, $\dot{\varphi}(t-\tau)$ and $\ddot{\varphi}(t-\tau)$ are denoted by φ_τ, $\dot{\varphi}_\tau$ and $\ddot{\varphi}_\tau$, respectively, hereinafter. The dynamics of the quiet standing process is governed by the following second-order nonlinear NDDE:

$$J_A\ddot{\varphi} + b_t\dot{\varphi} + k_t\varphi - mgl\sin\varphi = -\alpha\tanh\left(\frac{1}{\alpha}(K_p\varphi_\tau + K_d\dot{\varphi}_\tau + K_a\ddot{\varphi}_\tau)\right), \tag{2.6}$$

where the nonlinearity arises due to two reasons: (i) mechanical nonlinearity as expressed by the sin function; (ii) control nonlinearity as denoted by the tangent hyperbolic function. This delay differential equation is of neutral type because time delay also appears in the argument of the highest (i.e. of the second) derivative of the body angle.

3. Linear stability of quiet standing and parameter selection

The trivial solution $\varphi \equiv 0$ of the nonlinear NDDE (2.6) corresponds to the desired equilibrium of quiet standing. First, local stability is analysed by means of the linearized system

$$J_A\ddot{\varphi} + b_t\dot{\varphi} + k_t\varphi - mgl\varphi = -K_p\varphi_\tau - K_d\dot{\varphi}_\tau - K_a\ddot{\varphi}_\tau. \tag{3.1}$$

This is further simplified to the form

$$\ddot{\varphi} + b\dot{\varphi} - a\varphi = -P\varphi_\tau - D\dot{\varphi}_\tau - A\ddot{\varphi}_\tau, \tag{3.2}$$

with new system parameters

$$b = \frac{b_t}{J_A} \quad \text{and} \quad a = \frac{(mgl - k_t)}{J_A} > 0 \tag{3.3}$$

and new gain parameters

$$P = \frac{K_p}{J_A}, \quad D = \frac{K_d}{J_A} \quad \text{and} \quad A = \frac{K_a}{J_A}. \tag{3.4}$$

The positiveness of a is emphasized as it was shown in [36] that the upright position of the body is unstable without control (that is when $P = 0$, $D = 0$, $A = 0$) due to the fact that the passive stiffness k_t is less than the gravitational moment mgl. As the contribution of the passive damping is usually small, it is assumed to be negligible in further analysis: $b_t \approx 0$, i.e. $b \approx 0$.

The characteristic function of the linear NDDE (3.2) reads

$$D(\lambda) = \lambda^2 - a + (P + D\lambda + A\lambda^2)\,e^{-\lambda\tau}. \tag{3.5}$$

If $P \le a$, the characteristic equation $D(\lambda) = 0$ has at least one non-negative real characteristic root, which indicates that the linear system is not asymptotically stable for any combination of the control parameters D and A [4,38]. Furthermore, if $|A| > 1$, then $D(\lambda) = 0$ has infinitely many characteristic roots with positive real parts and the linear system is always unstable [39]. Therefore, only the case $P > a$ and $|A| < 1$ is considered hereafter.

At the limit of stability, there exists a critical characteristic root $\lambda = i\omega_c$ with ω_c referring to the critical angular frequency of the arising oscillation which is the sway of the human body. The decomposition of the characteristic function at this critical characteristic root yields the real and imaginary parts, respectively, as follows:

$$\mathrm{Re}(D(i\omega_c)) = (P - A\omega_c^2)\cos\omega_c\tau + D\omega_c\sin\omega_c\tau - \omega_c^2 - a \tag{3.6}$$

and

$$\mathrm{Im}\,(D(i\omega_c)) = (A\omega_c^2 - P)\sin\omega_c\tau + D\omega_c\cos\omega_c\tau + b\omega_c. \tag{3.7}$$

The equations $\mathrm{Re}(D(i\omega_c)) = 0$ and $\mathrm{Im}(D(i\omega_c)) = 0$ lead to

$$\sin\omega_c\tau = \frac{\omega_c D(\omega_c^2 + a)}{(\omega_c^2 A - P)^2 + \omega_c^2 D^2} > 0 \tag{3.8}$$

and

$$\cos\omega_c\tau = -\frac{\omega_c^4 A + (aA - P)\omega_c^2 - aP}{(\omega_c^2 A - P)^2 + \omega_c^2 D^2}. \tag{3.9}$$

Eliminating the harmonic terms yields a quartic algebraic equation in ω_c:

$$F(\omega_c) := (1 - A^2)\omega_c^4 + (2a - 2AP - D^2)\omega_c^2 + a^2 - P^2 = 0. \tag{3.10}$$

For $|A| < 1$, the only positive root of equation (3.10) is

$$\omega_c = \sqrt{\frac{-(2a - 2AP - D^2) + \sqrt{(2a - 2AP - D^2)^2 - 4(a^2 - P^2)(1 - A^2)}}{2(1 - A^2)}}. \tag{3.11}$$

The critical values of the time delay τ_c for possible stability switches can be expressed from (3.9) as a function of

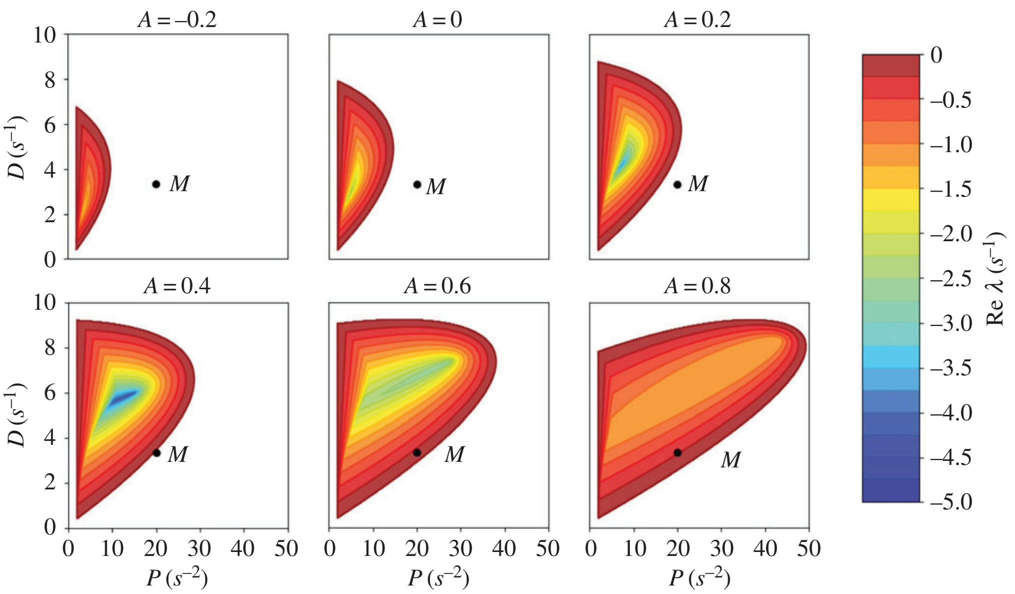

Figure 3. Stability charts for the control gains P, D and A with human system parameter $a = 2.15\ \mathrm{s}^{-2}$ and reaction delay $\tau = 0.2$ s. Contours refer to the strength of exponential decay in the stable domain. Point M represents biophysically plausible control parameters P and D. (Online version in colour.)

the other parameters:

$$\tau_{ck} = \frac{1}{\omega_c}\left[2k\pi + \arccos\left(-\frac{\omega_c^4 A + (aA - P)\omega_c^2 - aP}{(\omega_c^2 A - P)^2 + \omega_c^2 D^2}\right)\right],$$
$$k = 0, 1, \ldots. \tag{3.12}$$

Let γ_k denote the derivative of the characteristic root λ with respect to the time delay τ at its critical value τ_{ck}, i.e.

$$\gamma_k := \left.\frac{\mathrm{d}\lambda(\tau)}{\mathrm{d}\tau}\right|_{\tau=\tau_{ck}}. \tag{3.13}$$

The stability of equilibrium with respect to the time delay can be traced by means of the sign of the real part of γ_k (also called root tendency): if sgn(Re γ_k) is positive (negative), a pair of characteristic roots crosses the imaginary axis from left to right (right to left). According to the theory of stability switches [40], the system loses its stability when the delay reaches its first critical value at $k = 0$, because

$$\mathrm{sgn}(\mathrm{Re}\ \gamma_k) = \mathrm{sgn}\left.\frac{\mathrm{d}F}{\mathrm{d}\omega}\right|_{\omega=\omega_c} \tag{3.14}$$

for any non-negative integer k, where formula (3.10) gives

$$\left.\frac{\mathrm{d}F}{\mathrm{d}\omega}\right|_{\omega=\omega_c} = 2\omega_c\sqrt{(2a - 2AP - D^2)^2 - 4(a^2 - P^2)(1 - A^2)} > 0. \tag{3.15}$$

Consequently, Hopf bifurcation occurs already at the first critical value of the time delay defined by

$$\tau_c := \tau_{c0} = \frac{1}{\omega_c}\arccos\left(-\frac{\omega_c^4 A + (aA - P)\omega_c^2 - aP}{(\omega_c^2 A - P)^2 + \omega_c{+}^2 D^2}\right), \tag{3.16}$$

where ω_c is given in (3.11). At this point, the root tendency is

$$\gamma := \gamma_0$$
$$= \frac{-2\tau_c P - \mathrm{i}\omega_c\tau_c D + 2\tau_c a \mathrm{e}^{\mathrm{i}\omega_c\tau_c}}{-\tau_c{}^2 P + (1 - \mathrm{i}\omega_c\tau_c)\tau_c D + (2\mathrm{i} + \omega_c\tau_c)\omega_c\tau_c A + 2\mathrm{i}\omega_c\tau_c \mathrm{e}^{\mathrm{i}\omega_c\tau_c}}. \tag{3.17}$$

The use of acceleration feedback gain was proposed in [4] where several stability charts were constructed in the space of control parameters P, D and A for the biophysically plausible time delay and system parameters of human balancing. Figure 3 presents a series of similar stability charts in the (P, D) plane for varying acceleration gain $A \in [-0.2, 0.8]$. To study the balancing of inactive people, the reaction delay is fixed at $\tau = 0.2$ s. The system parameter $a = 2.15\ \mathrm{s}^{-2}$ comes from (3.3) with human weight $mg = 600$ N, mass moment of inertia $J_A = 60\ \mathrm{kg\,m}^2$ and passive stiffness $k_t = 471$ Nm rad^{-1} (for details see [6]).

The stability charts clearly show that increasing acceleration gain increases the stable region. The contour figures also provide additional information about the robustness properties in different aspects. On the one hand, the contour levels refer to different decay ratios of the oscillations scaled according to the largest (negative) real part of the characteristic roots; in this respect, the deep blue regions seem to be the most robust with respect to initial values and perturbations. On the other hand, the size and shape of the stable domains also indicate how robust the stability is with respect to control (or system) parameter uncertainties; for the corresponding robustness definitions see [39,41,42].

However, it is not the robustness considerations that determine primarily the choice of control parameters. Milton *et al.* [19] have shown in case of stick balancing experiments that control at the edge of stability minimizes the energetic costs. Manoeuvrability could also be maximized by tuning the parameters towards the edge of stability domains. The control parameters could be tuned into even slightly unstable regions where the sensory threshold (not considered in this study) helps to achieve micro-chaotic or long transient chaotic oscillations, which is satisfactory from practical balancing viewpoint [21]. All these considerations explain why the parameter point M in figure 3 is selected at $P = 20\ \mathrm{s}^{-2}$ and $D = 3.33\ \mathrm{s}^{-1}$ which correspond to the plausible gains $K_\mathrm{p} = 1200$ Nm rad^{-1} and $K_\mathrm{d} = 200$ Nms **Q1** rad^{-1} in accordance with (3.4) (see also [19,41,42]).

These parameters will be used when the results of the subsequent bifurcation analysis is discussed, while the acceleration gain A and the reaction delay τ will be still kept as varying parameters to study their role in the dynamics of

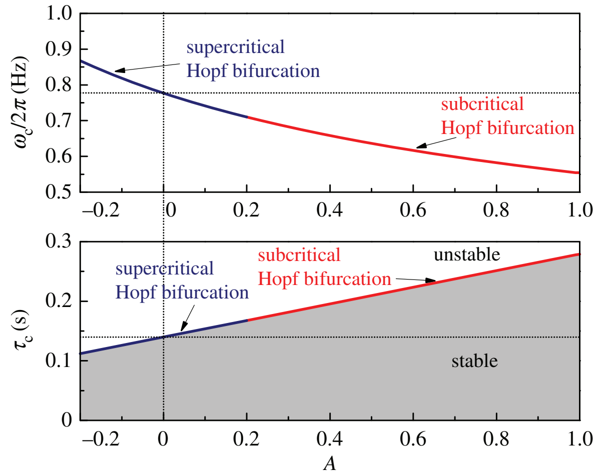

Figure 4. Critical time delays as a function of the acceleration gain A, the sense of Hopf bifurcation and the oscillation frequencies at loss of stability. Saturation limit $\alpha = 15$ Nm and other parameters are chosen at M in figure 3. (Online version in colour.)

Table 1. Nonlinear coefficients p_g and p_{hjk}.

p_{300}	$\frac{\tau_c^2 P^3 J_A^2}{3\alpha^2}$	p_{210}	$\frac{\tau_c P^2 D J_A^2}{\alpha^2}$
p_{201}	$\frac{P^2 A J_A^2}{\alpha^2}$	p_{120}	$\frac{P D^2 J_A^2}{\alpha^2}$
p_{111}	$\frac{2PDAJ_A^2}{\tau_c \alpha^2}$	p_{102}	$\frac{P A^2 J_A^2}{\tau_c^2 \alpha^2}$
p_{030}	$\frac{D^3 J_A^2}{3\tau_c \alpha^2}$	p_{021}	$\frac{D^2 A J_A^2}{\tau_c^2 \alpha^2}$
p_{012}	$\frac{D A^2 J_A^2}{\tau_c^3 \alpha^2}$	p_{003}	$\frac{A^3 J_A^2}{3\tau_c^4 \alpha^2}$
p_g		$-\frac{\tau_c^2 mgl}{6J_A}$	

balancing. The corresponding stability chart in the (A, τ) parameter plane is given in figure 4 together with critical oscillation frequencies ω_c at the loss of stability.

4. Nonlinear analysis

As the reaction delay (especially its processing component) strongly depends on the activity and awareness of human beings, the delay τ is one of the most varying human parameters. To analyse the effect of varying the delay on dynamics, the bifurcation parameter μ is chosen as

$$\tau = \tau_c + \mu \tag{4.1}$$

in the subsequent calculations where the critical delay τ_c is given in (3.16).

For small angular positions, we use the approximations

$$\sin\varphi \approx \varphi - \frac{1}{6}\varphi^3, \quad \tanh\varphi \approx \varphi - \frac{1}{3}\varphi^3 \tag{4.2}$$

and

$$\frac{1}{(\tau_c + \mu)^n} \approx \frac{1}{\tau_c^n} - \frac{n}{\tau_c^{n+1}}\mu. \tag{4.3}$$

By rescaling the time in the governing equation (2.6) as $\tilde{t} = t/\tau$ and dropping the tilde immediately for simplicity, one can get the third-order approximated nonlinear system in the form

$$\begin{aligned}\ddot{\varphi}(t) + A\ddot{\varphi}(t-1) + (\tau_c + \mu)D\dot{\varphi}(t-1) + (\tau_c{}^2 + 2\mu\tau_c)(P\varphi(t-1) - a\varphi(t))\\ = p_g\varphi(t)^3 + \sum_{h+j+k=3} p_{hjk}\varphi^h(t-1)\dot{\varphi}^j(t-1)\ddot{\varphi}^k(t-1),\end{aligned} \tag{4.4}$$

where p_g and p_{hjk} correspond to the third-order nonlinear geometric coefficient and the third-order nonlinear saturation coefficients. Their specific expressions are given in table 1.

The amplitude ρ of the bifurcated periodic motion satisfies

$$\rho = \sqrt{-8\frac{\mathrm{Re}\,\gamma}{\mathrm{Re}\,\Delta}(\tau - \tau_c)} + \text{h.o.t.}, \tag{4.5}$$

where the root tendency γ is calculated in (3.17), and the complex Poincaré–Lyapunov constant has the form

$$\Delta = \Delta_g + \Delta_s \tag{4.6}$$

with Δ_g and Δ_s separating the contribution of geometric nonlinearity and saturation nonlinearity, respectively:

$$\Delta_g = -\frac{mgl\,e^{i\omega_c\tau_c}\tau_c{}^2}{2J_A(-2\tau_c P - i\omega_c\tau_c D + 2\tau_c a e^{i\omega_c\tau_c})}\gamma \tag{4.7}$$

and

$$\Delta_s = \frac{J_A{}^2\tau_c{}^2(P^2 + \omega_c{}^2(D^2 - 2AP) + \omega_c{}^4A^2)(P + i\omega_c D - \omega_c{}^2A)}{\alpha^2(-2\tau_c P - i\omega_c\tau_c D + 2\tau_c a e^{i\omega_c\tau_c})}\gamma. \tag{4.8}$$

The calculations are carried out according to centre manifold reduction and normal form theory [43,44] and the algebraic results are confirmed with the method of multiple scales [45,46]. Both derivations are briefly summarized in the appendix.

For the biomechanically plausible parameter set introduced in §3, the above algebraic results of Hopf bifurcation analysis are presented with numerical values in table 2, with the sense of bifurcations in the stability chart of figure 4 and with the bifurcation diagrams in figures 5 and 6. The sign of the Poincaré–Lyapunov constant $\mathrm{Re}\,\Delta$ determines the sense of Hopf bifurcation: it is supercritical or subcritical if $\mathrm{Re}\,\Delta > 0$ or $\mathrm{Re}\,\Delta < 0$, respectively, i.e. the bifurcated periodic motions are stable or unstable, respectively.

The bifurcation diagrams are validated also by the numerical calculations of the stable and unstable periodic motions with the help of the collocation method combined with path-following techniques [47,48]. The corresponding numerical results are represented by circles in figures 5 and 6, and they show perfect agreement with the analytical results for small bifurcation parameter μ, i.e. close to the critical time delays τ_c. The minor deviations further away from the critical delays are the result of the third-order approximation used in the analytical calculations, while numerical ones use the original nonlinearity in the form of the tangent hyperbolic function in (2.4) and (4.2).

5. Discussion

In this section, the results of the linear stability analysis and the Hopf bifurcation calculations are discussed in detail as an attempt to interpret the role of acceleration feedback in human balance.

The analysis of stability switch with respect to time delay shows that the upright position loses its stability at the very

Table 2. Characteristic values and sense of Hopf bifurcations for different acceleration gains A in case of saturation limit $\alpha = 15$ Nm; other parameters are chosen at M in figure 3.

A	τ_c(s)	$\omega_c/2\pi$ (Hz)	Re γ (s^{-1})	Re Δ_g	Re Δ_s	Re Δ	sense
0	0.140	0.778	2.259	0.012	−656.488	−656.476	super
0.2	0.168	0.710	2.054	0.0001	−3.945	−3.945	super
0.4	0.196	0.659	1.866	−0.014	311.735	311.721	sub
0.6	0.223	0.617	1.693	−0.029	467.646	467.617	sub
0.8	0.251	0.583	1.535	−0.046	542.313	542.267	sub

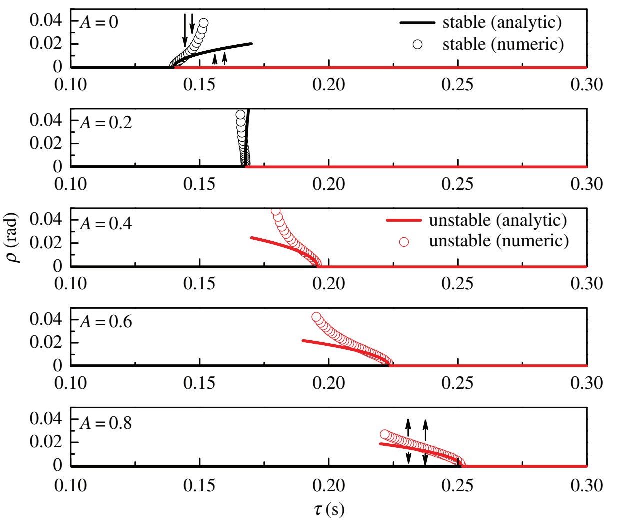

Figure 5. Bifurcation diagrams with respect to time delay for different acceleration gains A; data taken from table 2. Continuous lines refer to analytical results, series of circles refer to numerical results obtained by collocation method and path following. Black colour represents stable branches; red colour represents unstable branches. (Online version in colour.) Q2

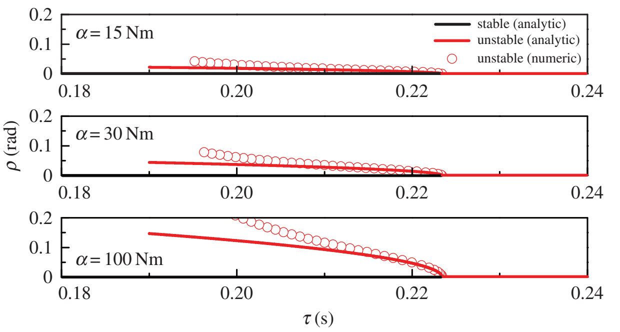

Figure 6. Bifurcation diagrams with respect to time delay for saturation limit α. The acceleration gain $A = 0.6$ and other parameters are chosen at M in figure 3. Continuous lines refer to analytical results, series of circles refer to numerical results obtained by collocation method and path following. Black/red represent stable/unstable branches. (Online version in colour.) Q2

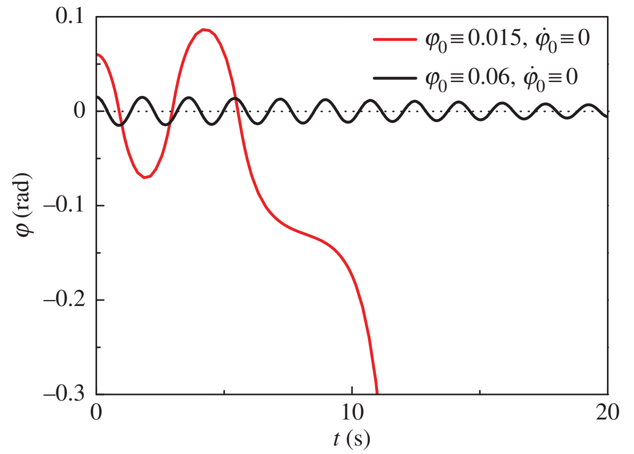

Figure 7. Time history with different initial conditions: $\varphi_0(t) \equiv 0.015$ rad $\approx 0.9^\circ$, $\dot\varphi_0(t) \equiv 0$ rad s^{-1}, $t \in [-\tau, 0]$ (black line) and $\varphi_0(t) \equiv 0.1$ rad $\approx 3.4^\circ$, $\dot\varphi_0(t) \equiv 0$ rad s^{-1}, $t \in [-\tau, 0]$ (red line). The acceleration gain $A = 0.6$, the reaction delay $\tau = 0.21\,\text{s} < 0.223\,\text{s} = \tau_c$ and other parameters are chosen at M in figure 3. (Online version in colour.) Q2

first critical time delay τ_c (see (3.16)) of the PDA controller. The positive effect of the acceleration feedback can be highlighted in two ways. On the one hand, the value of the critical reaction delay τ_c gets larger as acceleration gain A increases as shown in figure 4 for fixed position gain P and velocity gain D. On the other hand, the stable parameter region PD expands with increasing acceleration gain A as shown in figure 3 for fixed reaction delay τ. These figures not only confirm the stability results of [4], but also provide further validation of the mechanical model: at loss of stability, the oscillation frequencies in the range of 0.6–0.9 Hz (figure 4) describe a realistic sway of the human body in critical balancing situations. These slow oscillations are originated in the feedback control of the inverted pendulum as explained in [14]; other higher-frequency oscillations may exist due to errors in state estimation that is not studied here.

To interpret the nonlinear results, first, the physical meaning of the Hopf bifurcations is summarized briefly. In case of a supercritical Hopf bifurcation, small-amplitude stable oscillations appear around the upright position after linear stability is lost either by increased reaction delay or by mistuned control gains. This results in a tiny sway, which might be disturbing but the balancing is still practically successful, and no fall over occurs. The situation is much more dangerous in the case of subcritical Hopf bifurcations: the existence of small-amplitude unstable oscillations reduces the domain of attraction of the otherwise linearly stable controlled upright position. This means that for perturbations 'larger' than these unstable oscillations, the control is unable to stabilize the upright position anymore, which leads to fall over, in spite of the fact that the reaction delay and all the control parameters are tuned in the linearly stable domain. This phenomenon is a special case of finite-amplitude instabilities defined in a general context by Krechetnikov & Marsden [49].

The sense of the Hopf bifurcation is determined by the Poincaré–Lyapunov constant $\mathrm{Re}\,\Delta$, which is the sum of the geometry-related $\mathrm{Re}\,\Delta_g$ (see (4.7)) and the control saturation-related $\mathrm{Re}\,\Delta_s$ (see (4.8)). As the numerical values in table 2 show, the effect of geometric nonlinearity is negligible, because it is orders of magnitude smaller than the effect of the saturation nonlinearity. Consequently, $\Delta \approx \Delta_s$.

The results in table 2 and the corresponding stability and bifurcation diagrams in figures 4 and 5 can be interpreted in the following way. For a traditional PD controller, i.e. when $A = 0$, the stability is lost at the small value of reaction delay $\tau_c = 0.14$ s, but the Hopf bifurcation is supercritical (see similar results for robotic control in [25]). In other words, the human reaction delay is likely to be larger than the critical one leading to linear instability, but the body will sway with small amplitude only about the upright position. As figure 5 shows clearly, the increasing acceleration gain A pushes the appearance of the Hopf bifurcation for larger critical reaction delays, but in the mean time, it changes its sense to subcritical, and the amplitude of the unstable oscillation gets smaller and smaller, and the domain of attraction of stable balancing becomes narrower and narrower. This is represented by two time-domain simulation results in figure 7 for $A = 0.6$ and $\tau = 0.21\,\mathrm{s} < 0.223\,\mathrm{s} = \tau_c$. For a small perturbation given by the initial condition $\varphi_0(t) \equiv 0.015\,\mathrm{rad} \approx 0.9^\circ$, $\dot{\varphi}_0(t) \equiv 0\,\mathrm{rad\,s^{-1}}$, $t \in [-\tau, 0]$, the upright position is stabilized. However, for a larger perturbation like $\varphi_0(t) \equiv 0.06\,\mathrm{rad} \approx 3.4^\circ, \dot{\varphi}_0(t) \equiv 0\,\mathrm{rad\,s^{-1}}$, $t \in [-\tau, 0]$, the stability is lost after one sway that leads to fall over. Similar kind of 'hesitation' during fall over has already been observed in some of the video-recorded fall overs of inactive elderly people (see [3]).

Equation (4.8) shows that Δ_s has a reciprocal relationship with α^2, which means that the subcriticality of Hopf bifurcation becomes worse as the saturation torque α becomes smaller (figure 6). For elderly people, especially for inactive ones, the maximum active torque provided at the ankle could become very small, which means that already very small perturbations may destabilize them.

6. Conclusion

We have shown that the benefits of acceleration feedback in linear stabilization of quiet standing are limited due to the nonlinear saturation effect of the active control torque. Although the acceleration feedback improves the stability of equilibrium for increasing reaction delays, it deteriorates the robustness of stable balancing against perturbations as a result of the occurrence of subcritical Hopf bifurcations.

The delayed PDA controller is equivalent to a predictive controller where the actual state is predicted based on the delayed angular position, velocity and acceleration. With modelling the saturation of active control torque, an attempt was made to interpret the mechanism of fall over even when the reaction delay is smaller than the critical one. Although acceleration feedback increases the critical delay to quite a large extent, it does introduce subcritical Hopf bifurcation into the system, which leads to increased sensitivity for small perturbations. This sensitivity becomes even more critical as the maximum active torque levels at the ankle decrease for inactive ageing groups.

Data accessibility. All data are made available in the article.

Author's contributions. L.Z. derivation of the mathematical model, stability and bifurcation calculations, compilation of the main text, all formulae and figures of the report. G.S. basic concept of the project, construction of the mechanical model, structure of the manuscript, checking the calculations, corrections of text and figures, compilation of the Introduction. T.I. concept of the biomechanical elements of the balancing model, identification of control parameters, compilation of the biological meaning of the results, finalization of the manuscript.

Competing interests. We declare we have no competing interests.

Funding. The work of L.Z. was supported by the National Natural Science Foundation of China under Grants Nos. 11302098 and 11772151. The work of G.S. was also supported by the Research Fund of the State Key Laboratory of Mechanics and Control of Mechanical Structures (NUAA) under Grant No. MCMS-0116K01.

Acknowledgements. The authors acknowledge with thanks the discussions with Prof. John Milton (The Claremont Colleges). L.Z. gratefully acknowledges financial support from China Scholarship Council.

Appendix A

A.1. Centre manifold reduction combined with normal form calculation

The NDDE (4.4) at the critical delay τ_c, i.e. for $\mu = 0$, can be recast into the following form:

$$\frac{\mathrm{d}}{\mathrm{d}t}\boldsymbol{D}x_t = \boldsymbol{L}x_t + \boldsymbol{F}(x_t) + \boldsymbol{G}(x_t, \dot{x}_t), \tag{A 1}$$

where $\boldsymbol{x} = (x_1, x_2)^{\mathrm{T}} = (\varphi, \dot{\varphi})^{\mathrm{T}}$, $x_t(\theta) \equiv \boldsymbol{x}(t+\theta)$, $-1 \le \theta \le 0$, $x_t \in \boldsymbol{C} = \boldsymbol{C}([-1, 0], \mathbb{R}^2)$ is the Banach space of continuous functions from $[-1, 0]$ to $\mathbb{R}^2$ with the uniform norm, $\boldsymbol{D}$ and $\boldsymbol{L}$ are bounded linear operators from $\boldsymbol{C}$ to $\mathbb{R}^2$, $\boldsymbol{D}\boldsymbol{\phi} = \boldsymbol{\phi}(0) - \int_{-1}^{0} \mathrm{d}[\boldsymbol{\zeta}(\theta)]\boldsymbol{\phi}(\theta)$, $\boldsymbol{L}\boldsymbol{\phi} = \int_{-1}^{0} \mathrm{d}[\boldsymbol{\eta}(\theta)]\boldsymbol{\phi}(\theta)$, and $\boldsymbol{\eta}$ and $\boldsymbol{\zeta}$ are 2×2 matrix-valued functions of bounded variation defined on $[-1, 0]$. These matrices and operators take the actual form

$$\mathrm{d}\boldsymbol{\eta}(\theta) = \begin{bmatrix} 0 & \delta(\theta) \\ \tau_c^2(a\delta(\theta) - P\delta(\theta+1)) & -D\tau_c\delta(\theta+1) \end{bmatrix} \mathrm{d}\theta \tag{A 2}$$

and

$$\mathrm{d}\boldsymbol{\zeta}(\theta) = \begin{bmatrix} 0 & 0 \\ 0 & A\,\delta(\theta+1) \end{bmatrix} \mathrm{d}\theta, \tag{A 3}$$

with δ denoting the Dirac-δ function, and

$$\boldsymbol{D}x_t = \begin{bmatrix} x_1(t) \\ x_2(t) \end{bmatrix} + \begin{bmatrix} 0 & 0 \\ 0 & A \end{bmatrix} \begin{bmatrix} x_1(t-1) \\ x_2(t-1) \end{bmatrix} \tag{A 4}$$

and

$$\boldsymbol{L}x_t = \begin{bmatrix} 0 & 1 \\ a\tau_c{}^2 & 0 \end{bmatrix} \begin{bmatrix} x_1(t) \\ x_2(t) \end{bmatrix} + \begin{bmatrix} 0 & 0 \\ -P\tau_c{}^2 & -D\tau_c \end{bmatrix} \times \begin{bmatrix} x_1(t-1) \\ x_2(t-1) \end{bmatrix}. \tag{A 5}$$

The nonlinear terms are expressed as

$$\boldsymbol{F}(x_t) = \begin{bmatrix} 0 \\ p_g x_1^3(t) + \sum_{h+j=3} p_{hj0}\, x_1^h(t-1) x_2^j(t-1) \end{bmatrix} \tag{A 6}$$

and

$$\boldsymbol{G}(x_t, \dot{x}_t) = \begin{bmatrix} 0 \\ \sum\limits_{h+j+k=3k \neq 0} p_{hjk} x_1^h(t-1) x_2^j(t-1) \dot{x}_2^k(t-1) \end{bmatrix}. \tag{A 7}$$

The linearized part of equation (A 1) assumes the form

$$\frac{\mathrm{d}}{\mathrm{d}t}Dx_t = Lx_t. \tag{A 8}$$

Its solution defines a C^0 semigroup $T(t)$ on C, $T(t)\boldsymbol{\phi} = x_t(\boldsymbol{\phi})$, $t \geq 0$. The infinitesimal generator $\mathcal{A}$ associated with $T(t)$ is given by $\mathcal{A}\boldsymbol{\phi} = \dot{\boldsymbol{\phi}}$ and has domain

$$\mathrm{Dom}(\mathcal{A}) = \left\{ \boldsymbol{\phi} \in C\colon \frac{\mathrm{d}\boldsymbol{\phi}}{\mathrm{d}\theta} \in C, D\frac{\mathrm{d}\boldsymbol{\phi}}{\mathrm{d}\theta} = L\boldsymbol{\phi} \right\}. \tag{A 9}$$

The spectrum $\sigma(\mathcal{A})$ of $\mathcal{A}$ coincides with its point spectrum if and only if it satisfies the corresponding characteristic equation (3.5). Define $C^* = C([0,1], \mathbb{R}^{2*})$ where $\mathbb{R}^{2*}$ is the two-dimensional space of row vectors. Consider the adjoint bilinear form on $C^* \times C$:

$$\begin{aligned}(\boldsymbol{\psi},\boldsymbol{\phi}) = \boldsymbol{\psi}(0)D(\boldsymbol{\phi}) &- \int_{-1}^{0}\int_{0}^{\theta} \boldsymbol{\psi}(s-\theta)\mathrm{d}\boldsymbol{\eta}(\theta)\boldsymbol{\phi}(s)\mathrm{d}s \\ &+ \int_{1}^{0}\int_{0}^{\theta} \boldsymbol{\psi}'(s-\theta)\mathrm{d}\boldsymbol{\zeta}(\theta)\boldsymbol{\phi}(s)\mathrm{d}s.\end{aligned} \tag{A 10}$$

Let $\mathcal{A}^*$ denote the adjoint operator of $\mathcal{A}$ with respect to the bilinear form defined in equation (A 10), i.e., $\mathcal{A}^*{:}C^* \to C^*$, so that $(\boldsymbol{\psi}, \mathcal{A}\boldsymbol{\phi}) = (\mathcal{A}^*\boldsymbol{\psi}, \boldsymbol{\phi})$ holds for all $\boldsymbol{\phi} \in C$ and $\boldsymbol{\psi} \in C^*$. Let $\Lambda = \{\mathrm{i}\omega_c\tau_c, -\mathrm{i}\omega_c\tau_c\}$. There exists two subspace P_Λ and Q_Λ splitting of the space C, invariant under $T(t)$, such that $C = P_\Lambda \bigoplus Q_\Lambda$. A basis $\boldsymbol{\Phi}$ of P_Λ is given by

$$\Phi = [\boldsymbol{\phi}_1(\theta) \quad \boldsymbol{\phi}_2(\theta)], \tag{A 11}$$

where $\boldsymbol{\phi}_1(\theta) = (\mathrm{e}^{\mathrm{i}\omega_c\tau_c\theta}, \{\mathrm{i}\omega_c\mathrm{e}^{\mathrm{i}\omega_c\tau_c\theta}\})^{\mathrm{T}} = \overline{\boldsymbol{\phi}_2(\theta)}$, and a basis $\boldsymbol{\Psi}$ for Q_Λ can be expressed as

$$\Psi = \begin{bmatrix}\boldsymbol{\psi}_1(\xi) \\ \boldsymbol{\psi}_2(\xi)\end{bmatrix}, \tag{A 12}$$

where

$$\begin{aligned}\boldsymbol{\psi}_1(\xi) &= \left(\kappa\mathrm{e}^{-\mathrm{i}\omega_c\tau_c\xi}, \frac{1}{\mathrm{i}\mathrm{e}^{-\mathrm{i}\omega_c\tau_c}A\omega_c\tau_c + \mathrm{e}^{-\mathrm{i}\omega_c\tau_c}\tau_c D + \mathrm{i}\omega_c\tau_c}\kappa\mathrm{e}^{-\mathrm{i}\omega_c\tau_c\xi}\right) \\ &= \overline{\boldsymbol{\psi}_2(\xi)}\end{aligned}$$

in which

$$\kappa = \frac{\mathrm{i}\omega_c\tau_c A + D\tau_c + \mathrm{i}\omega_c\tau_c\mathrm{e}^{\mathrm{i}\omega_c\tau_c}}{A(\omega_c\tau_c)^2 + \mathrm{i}\omega_c\tau_c(2A - D\tau_c) + \tau_c(-P\tau_c + D) + 2\mathrm{i}\omega_c\tau_c\mathrm{e}^{\mathrm{i}\omega_c\tau_c}}, \tag{A 13}$$

satisfying $(\boldsymbol{\Psi}, \boldsymbol{\Phi}) = \boldsymbol{I}$. Also, $T(t)\boldsymbol{\Phi} = \boldsymbol{\Phi}\mathrm{e}^{Bt}$ where

$$B = \begin{bmatrix}\mathrm{i}\omega_c\tau_c & 0 \\ 0 & -\mathrm{i}\omega_c\tau_c\end{bmatrix}. \tag{A 14}$$

The infinitesimal generator $\mathcal{A}$ can be extended to an operator $\tilde{\mathcal{A}}$ by

$$\tilde{\mathcal{A}}\boldsymbol{\phi} = \mathcal{A}\boldsymbol{\phi} + X_0[L\boldsymbol{\phi} - D\boldsymbol{\phi}'], \quad \boldsymbol{\phi}' = \frac{\mathrm{d}\boldsymbol{\phi}}{\mathrm{d}\theta}, \tag{A 15}$$

onto the space BC, which is continuous on $[-1, 0)$ and with a possible finite jump discontinuity at 0. Functions $\boldsymbol{\psi}$ in BC can be represented as $\boldsymbol{\psi} = \boldsymbol{\phi} + X_0\boldsymbol{\beta}$, where $\boldsymbol{\phi} \in C$, $\boldsymbol{\beta} \in \mathbb{R}^2$, and

$$X_0(\theta) = \begin{cases}\mathbf{0} & -1 \leq \theta < 0, \\ \mathbf{I} & \theta = 0.\end{cases} \tag{A 16}$$

The bilinear form (A 10) can be extended to $C^* \times BC$ by setting $(\boldsymbol{\psi}, X_0) = \boldsymbol{\psi}(0)$.

With all these, the NDDE (4.4) can be expressed as the following abstract ordinary differential equation (ODE):

$$\dot{x}_t = \tilde{\mathcal{A}}x_t + X_0F(x_t) + X_0G(x_t, \dot{x}_t). \tag{A 17}$$

Let $\boldsymbol{\Pi}$: $BC \to P$ be the projection defined as $\boldsymbol{\Pi}(\boldsymbol{\phi} + X_0\boldsymbol{\zeta}) = \boldsymbol{\Phi}[(\boldsymbol{\Psi}, \boldsymbol{\phi}) + \boldsymbol{\Psi}(0)\boldsymbol{\zeta}]$. Then $BC = P \bigoplus \ker\boldsymbol{\Pi}$ and $Q \subset \ker\boldsymbol{\Pi}$, $x_t = \boldsymbol{\Phi}y(t) + z_t$ where $y(t) \in \mathbb{R}^2$, $z_t \in Q$. Then one can obtain the following decomposition of the neural system (A 17):

$$\dot{y} = By + \boldsymbol{\Psi}(0)(F(\boldsymbol{\Phi}y + z_t) + G(\boldsymbol{\Phi}y + z_t, \boldsymbol{\Phi}\dot{y} + \dot{z}_t)) \tag{A 18}$$

and

$$\dot{z}_t = \tilde{\mathcal{A}}z_t + (\mathbf{I} - \boldsymbol{\Pi})X_0(F(\boldsymbol{\Phi}y + z_t) + G(\boldsymbol{\Phi}y + z_t, \boldsymbol{\Phi}\dot{y} + \dot{z}_t)). \tag{A 19}$$

The normal form analysis is based on a recursive sequence of nonlinear transformations. As the non-resonance condition relative to Λ is satisfied, there exists a formal nonlinear transformation such that a local manifold satisfies $\tilde{z}_t = \mathbf{0}$ and the normal form on this invariant manifold yields the following two-dimensional ODE:

$$\begin{bmatrix}\dot{\tilde{y}}_1 \\ \dot{\tilde{y}}_2\end{bmatrix} = \begin{bmatrix}\mathrm{i}\omega_c\tau_c & 0 \\ 0 & -\mathrm{i}\omega_c\tau_c\end{bmatrix}\begin{bmatrix}\tilde{y}_1 \\ \tilde{y}_2\end{bmatrix} + \begin{bmatrix}\Delta\tilde{y}_1^2\tilde{y}_2 + \text{h.o.t.} \\ \bar{\Delta}\tilde{y}_1\tilde{y}_2^2 + \text{h.o.t.}\end{bmatrix}, \tag{A 20}$$

where Δ denotes the coefficient of $\tilde{y}_1^2\tilde{y}_2$ and h.o.t. stands for higher-order terms. According to the computation scheme proposed in [50], through recursive nonlinear transformations, the third-order normal form can be obtained. Through the following change of variables:

$$\begin{aligned}\tilde{y}_1 &= \frac{1}{2}(\rho\cos\phi - i\rho\sin\phi) \quad \text{and} \\ \tilde{y}_2 &= \frac{1}{2}(\rho\cos\phi + i\rho\sin\phi)\end{aligned} \tag{A 21}$$

equation (A 20) is transformed into the form:

$$\dot{\rho} = \frac{1}{8}\mathrm{Re}\,\Delta\rho^3 + \text{h.o.t.} \tag{A 22}$$

The unfolding takes the following form:

$$\dot{\rho} = \mathrm{Re}\,\gamma\rho\mu + \frac{1}{8}\mathrm{Re}\,\Delta\rho^3 + \text{h.o.t.}, \tag{A 23}$$

where γ and Δ are defined in (3.17) and (4.6). The amplitude formula (4.5) comes as a non-zero trivial solution of (A 23).

A.2. Calculation by the method of multiple scales

To study the small amplitude oscillation, let

$$\varphi(t) = \sqrt{\varepsilon}x(t) \quad \text{and} \quad \mu = \varepsilon\bar{\mu} \tag{A 24}$$

ε is a non-dimensional bookkeeping parameter, $0 < \varepsilon \ll 1$. $\bar{\mu} = \mathrm{O}(1)$ is the detuning parameter. Then equation (4.4) can be transformed into the form

$$\begin{aligned}&\ddot{x}(t) + A\ddot{x}(t-1) + \tau_c D\dot{x}(t-1) + \tau_c{}^2(Px(t-1) - ax(t)) \\ &\quad = -\varepsilon\bar{\mu}(D\dot{x}(t-1) - 2\tau_c(Px(t-1) - ax(t))) \\ &\qquad + \varepsilon(p_g x(t)^3 + \sum_{h+j+k=3} p_{hjk}x^h(t-1)\dot{x}^j(t-1)\ddot{x}^k(t-1)).\end{aligned} \tag{A 25}$$

The multiple timescales are defined as $T_k = \varepsilon^k t$, $r = 0, 1, 2, \ldots$. To study the Hopf bifurcation, a two-scale expansion of the solution is assumed as

$$x(t) = x_0(T_0, T_1) + \varepsilon x_1(T_0, T_1) + \mathrm{O}(\varepsilon^2). \tag{A 26}$$

By using the following differential operators [45]:

$$\frac{\mathrm{d}}{\mathrm{d}t} = \frac{\partial}{\partial T_0} + \varepsilon\frac{\partial}{\partial T_1} + O(\varepsilon^2) =: D_0 + \varepsilon D_1 + O(\varepsilon^2), \qquad \frac{\mathrm{d}^2}{\mathrm{d}t^2} =: {D_0}^2 + 2\varepsilon D_0 D_1 + O(\varepsilon^2), \tag{A 27}$$

the delayed terms can be expressed as

$$\begin{aligned} x(t-\tau) &= x_0(T_0-\tau, T_1-\varepsilon\tau) + \varepsilon x_1(T_0-\tau, T_1-\varepsilon\tau) + \cdots \\ &= x_0(T_0-\tau, T_1) + \varepsilon(x_1(T_0-\tau, T_1) - \tau D_1 x_0(T_0-\tau, T_1)) \\ &\quad + O(\varepsilon^2). \end{aligned} \tag{A 28}$$

Substituting equations (A 26), (A 27) and (A 28) into equation (A 25) and equating the same powers of ε, a set of linear partial differential equations can be obtained in the form

$$D_0^2 x_0 - a\tau_c^2 x_0 + P\tau_c^2 x_{0\tau} + D\tau_c D_0 x_{0\tau} + AD_0^2 x_{0\tau} = 0 \tag{A 29}$$

and

$$\begin{aligned} & D_0^2 x_1 - a\tau_c^2 x_1 + P\tau_c^2 x_{1\tau} + D\tau_c D_0 x_{1\tau} + AD_0^2 x_{1\tau} \\ &= (2\tau_c x_0 - 2P\tau_c x_{0\tau} - DD_0 x_{0\tau})\bar{\mu} + (P{\tau_c}^2 - D\tau_c)D_1 x_{0\tau} \\ &\quad - 2D_0 D_1 x_0 + AD_0^2 D_1 x_{0\tau} - 2AD_0 D_1 x_{0\tau} + D\tau_c D_0 D_1 x_{0\tau} \\ &\quad + p_{030}(D_0 x_{0\tau})^3 + (p_{021} D_0^2 x_{0\tau} + p_{210} x_{0\tau})(D_0 x_{0\tau})^2 \\ &\quad + (p_{012}(D_0^2 x_{0\tau})^2 + p_{111} x_{0\tau} D_0^2 x_{0\tau} + p_{210} {x_{0\tau}}^2) D_0 x_{0\tau} \\ &\quad + p_{102} x_{0\tau}(D_0^2 x_{0\tau})^2 + p_{201} {x_{0\tau}}^2 D_0^2 x_{0\tau} + p_{300} {x_{0\tau}}^3 \\ &\quad + p_{003}(D_0^2 x_{0\tau})^3 + p_g {x_0}^3, \end{aligned} \tag{A 30}$$

where $x_i = x_i(T_0, T_1)$, $x_{i\tau} = x_i(T_0-\tau, T_1)$, and p_{ijk}, p_g are defined in table 1.

At the stability boundary, only one pair of pure imaginary characteristic roots $\pm i\omega_c$ exists, while all other eigenvalues have negative real parts. All the solution terms related to these negative real eigenvalues decay with time. Thus, to study the long-time behaviour of the system, the solution of equation (eqn A 29) can be assumed as

$$x_1 = R(T_1)e^{i\omega_c\tau_c T_0} + \overline{R(T_1)}e^{-i\omega_c\tau_c T_0}. \tag{A 31}$$

Substituting equation (A 31) into equation (A 30), the secular term can be found:

$$\begin{aligned} & (-2P\tau_c - iD\omega_c\tau_c + 2a\tau_c e^{i\omega_c\tau_c})R\bar{\mu} + (3e^{i\omega_c\tau_c} p_g \\ &\quad - 3{\omega_c}^6{\tau_c}^6 p_{003} + i{\omega_c}^5{\tau_c}^5 p_{012} - {\omega_c}^4{\tau_c}^4(p_{021} - 3p_{102}) \\ &\quad + i{\omega_c}^3{\tau_c}^3(3p_{030} - p_{111}) + {\omega_c}^2{\tau_c}^2(p_{210} - 3p_{201}) \\ &\quad + i\omega_c\tau_c p_{210} + 3p_{300})R^2\bar{R} - \tau_c(-P\tau_c + D(1 - i\omega_c\tau_c) \\ &\quad + A\omega_c(2i + \omega_c\tau_c) + 2ie^{i\omega_c\tau_c}\omega_c)\dot{R} = 0. \end{aligned} \tag{A 32}$$

By substituting the parameters in table 1 into (A 32), $\dot{R}$ can be determined by

$$\dot{R} = \gamma R\bar{\mu} + \Delta R^2\bar{R}. \tag{A 33}$$

Having

$$\tilde{y}_1 = \frac{1}{\sqrt{\varepsilon}} Re^{i\omega_c t}, \tag{A 34}$$

the normal form equation (A 33) is transformed into the same form as the normal form equation (A 23) derived by using centre manifold reduction and normal form theory.

References

1. Stevens JA, Sogolow ED. 2005 Gender differences for non-fatal unintentional fall related injuries among older adults. *Inj. Prev.* **11**, 115–119. (doi:10.1136/ip.2004.005835)
2. Stevens JA, Corso PS, Finkelstein EA, Miller TR. 2006 The costs of fatal and non-fatal falls among older adults. *Inj. Prev.* **12**, 290–295. (doi:10.1136/ip.2005.011015)
3. Robinovitch SN, Feldman F, Yang Y, Schonnop R, Lueng PM, Sarraf T, Sims-Gould J, Loughin M. 2013 Video capture of the circumstances of falls in elderly people residing in long-term care: an observational study. *Lancet* **381**, 47–54. (doi:10.1016/S0140-6736(12)61263-X)
4. Insperger T, Milton JG, Stepan G. 2013 Acceleration feedback improves balancing against reflex delay. *J. R. Soc. Interface* **10**, 20120763. (doi:10.1098/rsif.2012.0763)
5. Stepan G. 2009 Delay effects in brain dynamics. *Phil. Trans. R. Soc. A* **367**, 1059–1062. (doi:10.1098/rsta.2008.0279)
6. Asai Y, Tasaka Y, Nomura K, Nomura T, Casadio M, Morasso P. 2009 A model of postural control in quiet standing: robust compensation of delay-induced instability using intermittent activation of feedback control. *PLoS ONE* **4**, e6169. (doi:10.1371/journal.pone.0006169)
7. Milton JG, Townsend JL, King MA, Ohira T. 2009 Balancing with positive feedback: the case for discontinuous control. *Phil. Trans. R. Soc. A* **367**, 1181–1193. (doi:10.1098/rsta.2008.0257)
8. Cabrera JL, Milton JG. 2002 On-off intermittency in a human balancing task. *Phys. Rev. Lett.* **89**, 158702. (doi:10.1103/PhysRevLett.89.158702)
9. Loram ID, Maganaris CN, Lakie M. 2005 Human postural sway results from frequent, ballistic bias impulses by soleus and gastrocnemius. *J. Physiol.* **564**, 295–311. (doi:10.1113/jphysiol.2004.076307)
10. Peterka RJ. 2003 Simplifying the complexities of maintaining balance. *IEEE Eng. Med. Biol. Mag.* **22**, 63–68. (doi:10.1109/memb.2003.1195698)
11. Nijhawan R. 2008 Visual prediction: psychophysics and neurophysiology of compensation for time delays. *Behav. Brain Sci.* **31**, 179–198. (doi:10.1017/S0140525X08003804)
12. Stepan G. 2009 Delay effects in the human sensory system during balancing. *Phil. Trans. R. Soc. A* **367**, 1195–1212. (doi:10.1098/rsta.2008.0278)
13. Milton JG, Luis Cabrera J, Ohira T, Tajima S, Tonosaki Y, Eurich CW, Campbell SA. 2009 The time-delayed inverted pendulum: implications for human balance control. *Chaos* **19**, 026110. (doi:10.1063/1.3141429)
14. Kiemel T, Oie KS, Jeka JJ. 2006 Slow dynamics of postural sway are in the feedback loop. *J. Neurophysiol.* **95**, 1410–1418. (doi:10.1152/jn.01144.2004)
15. Li Y, Levine WS, Loeb GE. 2012 A two-joint human posture control model with realistic neural delays. *IEEE Trans. Neural. Syst. Rehabil. Eng.* **20**, 738–748. (doi:10.1109/tnsre.2012.2199333)
16. Wiesmeier IK, Dalin D, Maurer C. 2015 Elderly use proprioception rather than visual and vestibular cues for postural motor control. *Front. Aging Neurosci.* **7**, 97. (doi:10.3389/fnagi.2015.00097)
17. Yeh TT, Cluff T, Balasubramaniam R. 2014 Visual reliance for balance control in older adults persists when visual information is disrupted by artificial feedback delays. *PLoS ONE* **9**, e91554. (doi:10.1371/journal.pone.0091554)
18. Hick WE. 1952 On the rate of gain of information. *Q. J. Exp. Psychol.* **4**, 11–26. (doi:10.1080/17470215208416600)
19. Milton J, Meyer R, Zhvanetsky M, Ridge S, Insperger T. 2016 Control at stability's edge minimizes energetic costs: expert stick balancing. *J. R. Soc. Interface* **13**, 20160212. (doi:10.1098/rsif.2016.0212)
20. Haller G, Stepan G. 1996 Micro-chaos in digital control. *J. Nonlinear Sci.* **6**, 415–448. (doi:10.1007/BF02440161)

21. Stepan G, Milton J, Insperger T. 2017 Quantization improves stabilization of dynamical systems with delayed feedback. *Chaos* **13**, 114306. (doi:10.1063/1.5006777)
22. Bingham JT, Choi JT, Ting LH. 2011 Stability in a frontal plane model of balance requires coupled changes to postural configuration and neural feedback control. *J. Neurophysiol.* **106**, 437–448. (doi:10.1152/jn.00010.2011)
23. Kowalczyk P, Glendinning P, Brown M, Medrano-Cerda G, Dallali H, Shapiro J. 2012 Modelling human balance using switched systems with linear feedback control. *J. R. Soc. Interface* **9**, 234–245. (doi:10.1098/rsif.2011.0212)
24. Paoletti P, Mahadevan L. 2012 Balancing on tightropes and slacklines. *J. R. Soc. Interface* **9**, 2097–2108. (doi:10.1098/rsif.2012.0077)
25. Habib G, Rega G, Stepan G. 2015 Stability analysis of a two-degree-of-freedom mechanical system subject to proportional-derivative digital position control. *J. Vib. Control* **21**, 1539–1555. (doi:10.1177/1077546312474014)
26. Samad T. 2017 A Survey on industry impact and challenges thereof. *IEEE Control Sys. Magzine* **2**, 17–18. (doi:10.1109/MCS.2016.2621438)
27. Gu K, Niculescu S. 2003 Survey on recent results in the stability and control of time-delay systems. *J. Dyn. Sys. Meas. Control* **2**, 158–165. (doi:10.1115/1.1569950)
28. Wang ZH, Xu Q. 2017 Sway reduction of a pendulum on a movable support using a delayed proportional-derivative or derivative-acceleration feedback. *Procedia IUTAM* **22**, 176–183. (doi:10.1016/j.piutam.2017.08.024)
29. Baloh RW, Honrubia V. 1990 *Clinical neurology of the vestibular system*. Philadelphia.
30. Proske U, Gandevia SC. 2012 The proprioceptive senses: their roles in signaling body shape, body position and movement, and muscle force. *Physiol. Rev.* **92**, 1651–1697. (doi:10.1152/physrev.00048.2011)
31. Fallon JB, Bent LR, McNulty PA, Macefield VG. 2005 Evidence for strong synaptic coupling between single tactile afferents from the sole of the foot and motoneurons supplying leg muscles. *J. Neurophysiol.* **94**, 3795–3804. (doi:10.1152/jn.00359.2005)
32. Milton , Gyorffy J, Cabrera JL, Ohira T. 2010 Amplitude control of human postural sway using achilles tendon vibration. *16th US National Congress of Theoretical and Applied Mechanics*, Pennsylvania, USA.
33. Kapitza PL. 1951 Dynamic stability of a pendulum when its point of suspension vibrates. *Soviet Phys. JETP* **21**, 588–592.
34. Zelei A, Stepan G. 2008 The influence of parametric excitation on floating bodies. *Proc. Appl. Math. Mech.* **8**, 10 929–10 930. (doi:10.1002/pamm.200810929)
35. Insperger T. 2011 Stick balancing with reflex delay in case of parametric forcing. *Commun. Nonlinear Sci. Numer. Simul.* **16**, 2160–2168. (doi:10.1016/j.cnsns.2010.07.025)
36. Loram ID, Lakie M. 2002 Direct measurement of human ankle stiffness during quiet standing: the intrinsic mechanical stiffness is insufficient for stability. *J. Physiol.* **545**, 1041–1053. (doi:10.1113/jphysiol.2002.025049)
37. Vette AH, Masani K, Nakazawa K, Popovic MR. 2010 Neural-mechanical feedback control scheme generates physiological ankle torque fluctuation during quiet stance. *IEEE Trans. Neural. Syst. Rehabil. Eng.* **18**, 86–95. (doi:10.1109/tnsre.2009.2037891)
38. Stepan G. 1989 *Retarded dynamical systems: stability and characteristic functions*. New York, NY: Longman Group.
39. Michiels W, Niculescu S. 2007 *Stability and stabilization of time-delay systems: an eigenvalue-based approach*. Philadelphia, PA: SIAM.
40. Hu HY, Wang ZH. 2002 *Dynamics of controlled mechanical systems with delayed feedback*. Berlin: Springer.
41. Bingham JT, Ting LH. 2013 Stability radius as a method for comparing the dynamics of neuromechanical systems. *IEEE Trans. Neural Syst. Rehabil. Eng.* **21**, 840–848. (doi:10.1109/TNSRE.2013.2264920)
42. Hajdu D, Milton J, Insperger T. 2016 Extension of stability radius to neuromechanical systems with structured real perturbations. *IEEE Trans. Neural Syst. Rehabil. Eng.* **24**, 1235–1242. (doi:10.1109/TNSRE.2016.2541083)
43. Faria T, Magalhaes LT. 1995 Normal forms for retardee functional differential equaitons with parameters and applications to Hopf singularity. *J. Differ. Equ.* **122**, 181–200. (doi:10.1006/jdeq.1995.1144)
44. Weedermann M. 2001 Normal formal for neutral functional differential equations. *Fields Inst. Commun.* **29**, 361–368.
45. Nayfeh AH, Mook DT. 1979 *Nonlinear osillations*. New York, NY: Wiley.
46. Nayfeh AH. 2008 Order reduction of retarded nonlinear systems-the method of multiple scales versus center-manifold reduction. *Nonlinear Dyn.* **51**, 483–500. (doi:10.1007/s11071-007-9237-y)
47. Barton DAW, KrauskopF B, Wilson RE. 2006 Collocation schemes for periodic solutions of neutral delay differential equations. *J. Differ. Equ. Appl.* **12**, 1087–1101. (doi:10.1080/10236190601045663)
48. Engelborghs K, Luzyanina T, Samaey G. 2001 DDE-BIFTOOL v. 2.00: A Matlab Package for Bifurcation Analysis of Delay Differential Equations.
49. Krechetnikov R, Marsden JE. 2009 On the origin and nature of finite-amplitude instabilities in physical systems. *J. Phys. A: Math. Theor.* **42**, 412004. (doi:10.1088/1751-8113/42/41/412004)
50. Zhang L, Wang HL, Hu HY. 2012 Symbolic computation of normal form for Hopf bifurcation in a neutral delay differential equation and an application to a controlled crane. *Nonlinear Dyn.* **70**, 463–473. (doi:10.1007/s11071-012-0468-1)